PCCP

Volume 1 | Number 1 | Jan 2013 | Pages 1–100

PCCP

Physical Chemistry Chemical Physics
www.rsc.org/pccp

ROYAL SOCIETY OF CHEMISTRY

This is an *Accepted Manuscript*, which has been through the Royal Society of Chemistry peer review process and has been accepted for publication.

Accepted Manuscripts are published online shortly after acceptance, before technical editing, formatting and proof reading. Using this free service, authors can make their results available to the community, in citable form, before we publish the edited article. We will replace this *Accepted Manuscript* with the edited and formatted *Advance Article* as soon as it is available.

You can find more information about *Accepted Manuscripts* in the **Information for Authors**.

Please note that technical editing may introduce minor changes to the text and/or graphics, which may alter content. The journal's standard **Terms & Conditions** and the **Ethical guidelines** still apply. In no event shall the Royal Society of Chemistry be held responsible for any errors or omissions in this *Accepted Manuscript* or any consequences arising from the use of any information it contains.

ROYAL SOCIETY OF CHEMISTRY

www.rsc.org/pccp

Journal Name

ARTICLE

Anion and Cation Effects on Size Control of Au Nanoparticles Prepared by Sputter Deposition in Imidazolium-based Ionic Liquids[†]

Yoshikiyo Hatakeyama,[‡a] Ken Judai,[a] Kei Onishi,[b] Satoshi Takahashi,[b] Satoshi Kimura,[b] and Keiko Nishikawa*[b]

The sputter deposition of metal in an ionic liquid (IL) capture medium is a simple and elegant method for preparing nanoparticles without any chemical reaction. Although there have been some reports on the size determination factors for Au nanoparticles (AuNPs) prepared using this method, the effects with respect to the type of ILs used have not been clearly elucidated. This is because there are some complicating factors, some of which have been revealed by our previous systematic studies. In the present study, we prepare AuNPs in nine types of imidazolium-based ILs to examine the size determination effects of the type of anion involved, the length of the alkyl chain of the cation, and the preparation temperature for each IL, while keeping other factors constant. For most of the capture media ILs, the sizes of the AuNPs increase with an increase in temperature. The AuNPs prepared in ILs containing different types of anions exhibit distinctly different particle sizes and temperature dependences. Conversely, the alkyl chain is regarded a secondary stabilizer that works only at higher preparation temperatures. We conclude that the sizes of AuNPs prepared by this method may be determined by the competition between the collision frequency of the ejected Au atoms and the stabilizing capability of the anions that form the first coordination shell around the AuNPs. The AuNP sizes are closely related to the volume of anions.

1 Introduction

Owing to their unique properties, metal nanoparticles (NPs) have attracted a great deal of attention as functionalized materials for use in optical devices,[1–3] electrical devices,[4,5] biosensors,[3,6] and catalysts.[7–9] Because their properties and functions are strongly dependent on the size and shape of the NPs used,[10] the development of techniques for synthesizing size- and shape-controlled NPs is very important.

Whereas wet processes are typical in the chemical synthesis of metal/alloy NPs by reductive methods not only in general liquids[4,10,11] but also in ionic liquids (ILs),[12–19] other physical processes that offer unique and simple methods for generating metal/alloy NPs in ILs[20,21] have attracted much attention. In these methods, atoms, clusters, or fragments of metals are ejected by sputtering,[22–25] thermal evaporation,[26–28] or laser ablation[29,30] from bulk metals, and are then captured

a. College of Humanities and Sciences, Nihon University, Sakurajosui, Setagaya-ku, Tokyo 156-8550, Japan
b. Graduate School of Advanced Integration Science, Chiba University, Yayoi-cho, Inage-ku, Chiba 263-8522, Japan
†Electronic Supplementary Information (ESI) available: This section includes the TEM images, the UV–Vis spectra, the intensities and curve-fitting results of the SAXS profiles, and the densities and viscosities of the ILs used to prepare the AuNPs. See DOI: 10.1039/x0xx00000x
‡Present Address: Graduate School of Advanced Integration Science, Chiba University, Yayoi-cho, Inage-ku, Chiba 263-8522, Japan
*E-mail: k.nishikawa@faculty.chiba-u.jp

in a medium to form NPs. Except for laser ablation, the capture media used for this purpose must have low vapor pressure to endure vacuum operation. Moreover, if the medium has a stabilizing ability to prevent NPs from aggregating, clean NPs can be generated in the medium without any chemical reaction or additional stabilizing agents.

Among these physical preparation methods, the combination of sputtering to generate atoms or small clusters and deposition in an IL as the capture medium is a highly elegant method from the viewpoint of the possibility of generating sub-10-nm NPs of relatively uniform sizes. The vapor pressures of most ILs, if any, are negligibly small.[31,32] When ILs are used as capture media, complicated devices[33–35] are unnecessary and metal NPs are obtained through a very simple operation. Moreover, because the constituent ions of ILs stabilize the generated NPs,[36,37] no additional stabilizing agents are needed. Because the first report of the use of the sputter-deposition technique with ILs as the capture media for NPs synthesis,[22] many investigations[23–25,38–44] have been conducted to develop preparative techniques and to elucidate the formation mechanisms and factors that determine the size and shape of NPs. Moreover, some groups have applied the results to various nonvolatile liquids such as functionalized ILs,[45,46] castor oil,[47] and low-molecular-weight polymers.[48–52]

In this study, we limit our subject to Au nanoparticles (AuNPs) synthesized by the sputter deposition-technique in imidazolium-based ILs. In the first report on this method,

Torimoto et al. showed that the sizes of AuNPs are dependent on the type of IL.[22] Subsequently, although some groups have reported the size and size distribution of metal NPs in various ILs,[40,42–44,46] the values have not been consistent even when using the same capture medium. This confusion has occurred because of the many complicating inter-related factors.

We have performed a number of systematic studies to identify the factors that determine the size and size distribution of AuNPs. First, we reported that they are affected by the alkyl-chain length of the cation.[40] Second, we found that they are highly controlled by the temperature of the capture medium.[42] From these results, we concluded that the collision of the ejected metal particles determines the size and size distribution of NPs generated by sputter deposition and that the alkyl chains of cations play the role of stabilization agents. Although it has been reported that post heat-treatments cause the aggregation of once generated NPs and result in the formation of larger NPs,[38,41,42] the temperature effects, which we discuss here, are those relating to the nucleation and growth of AuNPs at the time of the sputter-deposition operation. The other important factors that determine the size and size distribution of NPs are the sputtering conditions. In a recent study, we generated AuNPs while systematically varying these conditions to elucidate their effects and concluded that the temperature of the target and the applied voltages strongly influence the size of the AuNPs generated in the capture media, while the working distance between the target and the surface of the capture media, the sputtering time, the discharge current, and the gas pressure have little or no influence.[44] As a result of these investigations of the size-control factors, we then prepared AuNPs 0.8 to 4.8 nm in size and reported the size-dependence of the microscopic structures.[53]

With respect to the size-control of AuNPs generated by the sputter-deposition technique in ILs, the effect of the anion is unresolved. Moreover, we must revisit the effect of the alkyl-chain length of the cation, which changes depending on the temperature. As mentioned above, some groups have investigated how the type of ion influences the size of NPs. However, including our first study on the effect of alkyl-chain length,[40] no attention has been directed to factors other than the type of ion. The answer is thought to involve many intricate factors. Now at last, our systematic studies on the factors affecting NP size control[42,44] have made it possible to extract the effects originating only from the anions and cations of the capture media ILs. The present study is intended to be a decisive report on the anion and cation effects on the size control of AuNPs generated by sputter deposition in imidazolium-based ILs.

There are three well-known methods for structurally characterizing AuNPs: ultraviolet–visible (UV–Vis) absorption spectroscopy, transmission electron microscopy (TEM), and small-angle X-ray scattering (SAXS). We mainly applied SAXS to obtain the size distributions of the prepared AuNPs because it is the most adequate and simplest method for the samples used in this study, as described in our previous studies.[40,42,44]

2 Experimental

2.1 ILs as Capture Media

We limited our samples to Au for the NPs and to typical imidazolium-based ILs for the capture media. To elucidate the anion effects in controlling the size of AuNPs, we selected five types of fluorine-containing anions, tetrafluoroborate (BF_4^-), hexafluorophosphate (PF_6^-), trifluoromethylsulfonate ([OTf]$^-$), bis(fluorosulfonyl)amide ([FSA]$^-$), and bis(trifluoromethanesulfonyl)amide ([TFSA]$^-$), and set 1-butyl-3-methylimidazolium ([C_4mim]$^+$) as the counter cation. To investigate the cation effects, the effects of the alkyl-chain length in particular, we selected four types of imidazolium-based cations with different alkyl chains to fix the anion of BF_4^- or [OTf]$^-$; namely, the 1-ethyl-3-methylimidazolium ([C_2mim]$^+$), [C_4mim]$^+$, 1-hexyl-3-methylimidazolium ([C_6mim]$^+$), and 1-methyl-3octylimidazolium ([C_8mim]$^+$) cations. Hereafter, we abbreviate these ILs as [$C_n$mim]BF_4 (n = 2, 4, 8), [C_4mim]PF_6, [$C_n$mim][OTf] (n = 2, 4, 6), [C_4mim][FSA], and [C_4mim][TFSA]. Schematics of the structures of the five anions and the [C_4mim]$^+$ cation are shown in Fig. 1. The optimized ion structures at the ground state were calculated based on the density functional theory at the B3LYP/6-311++G(d,p)[54,55] level of theory using the Gaussian 09 program package.[56] All the samples except the [OTf]$^-$ salts and [C_8mim]BF_4 were purchased from Kanto Chemical Co. Inc. They were all colorless, and their purities were guaranteed to be higher than 98%. Three types of [OTf]$^-$ salts and the [C_8mim]BF_4 were purchased from Merck and Wako Pure Chemical Industries, respectively. Their purities were also guaranteed to be higher than 98%.

For most ILs, the presence of adventitious water greatly affects their physical and chemical properties.[57–59] Therefore, all samples were dried for 24 h at 333 K under a vacuum of approximately 10^{-3} Pa and then kept under an argon
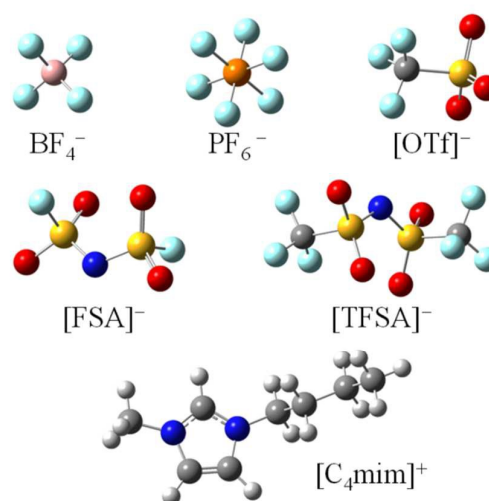
Fig. 1 Structures of the five anions and the [C_4mim]$^+$. The aqua, pink, orange, gray, yellow, red, blue, and white spheres represent F, B, P, C, S, O, N, and H atoms, respectively.

atmosphere before sputter deposition. The water content of each sample was determined by Karl Fischer titration (DL32, Mettler Toledo International) and was less than 40 ppm. The purity of the Au target from Tanaka Kikinzoku Kogyo K.K. was 99.99 %.

2.2 Sputter Deposition of Au onto the Capture Media

A schematic diagram of our sputter-deposition apparatus was shown in our previous paper.[44] The main characteristics of the apparatus were a temperature-regulating device for the capture medium and a cooling device for the Au target. The two devices were attached to a commercially available sputter coater (SC-704, SANYU Electron Co. Ltd.). The former device, which circulates temperature-regulated water around the base of the chamber, helped to maintain a constant temperature of the capture medium in the range of 20–80 °C, within ±1 °C, during sputter deposition. By attaching the cooling water-circulating device to the target, the temperature of the target was maintained at 20 °C. If the circulation of cooled water was stopped, the temperature would exceed 100 °C during the sputtering operation and the temperature increase in the target would significantly influence the form of the sputtered Au.

We spread an IL (2 cm^3) on a horizontal stainless plate (15.9 cm^2) in the sputter coater. A 25 mm working distance between the Au target and the liquid surface was maintained. The sputtering time was 50 min. The Au concentration was nearly proportional to the sputtering time. Under these conditions, the concentration of Au atoms was estimated from density measurements to be approximately 40 mmol/dm^3. The applied voltage and discharge current were set at 1.0 kV and 20 mA, respectively. By the applied voltage and discharged current in our apparatus, the Ar pressure was consistently determined to be 12–14 Pa.

AuNPs were prepared in each IL sample, while the temperature was increased from 20 °C to 80 °C in 10 °C intervals within the margin of ±1 °C, and the temperature of Au target was maintained at 20 °C during sputtering.

2.3 SAXS Measurements

To characterize the size and size distribution of the AuNPs immediately after AuNP generation, we measured the SAXS intensities using a SAXS apparatus (NANO-Viewer, RIGAKU Corporation). To obtain precise SAXS intensity data, some devices were attached to the commercially available SAXS apparatus. These details, as well as our experimental procedures, are described in our previous studies.[40,42]

Each sample was packed in a holder with windows of polyetherimide thin film (SUPERIO UT F type: Mitsubishi Plastics, Inc.) immediately after preparation by sputter deposition. The sample holder had an inside diameter of 6 mm and a thickness of 0.3 mm. The thickness was adjusted with a Teflon spacer. Because of the hygroscopic property of the ILs, all sampling operations were performed under an Ar atmosphere. The SAXS measurement for each sample was performed at room temperature because NPs generated at higher temperatures have been ascertained to keep their original size and shape during the cooling operation.

The theoretical curves of the measured SAXS intensities were fitted under the assumption that the NPs are spherical, and the size distribution is expressed by a Γ distribution. Further details are given in our previous paper.[40] From this analysis, we extracted two parameters—the value of the diameter at the peak (D_{peak}), which corresponds to the diameter of the most abundant NPs and the full width at half maxima (W_{fwhm}) of the distribution curves.

2.4 TEM and UV–Vis Spectrum Measurements

To roughly assess the size and shape of the prepared particles, two samples, AuNPs prepared in [C$_4$mim]BF$_4$ at 60 °C and [C$_4$mim][TFSA] at 30 °C, were observed with a TEM apparatus (JEM-3100FEF, JEOL Ltd.) having an acceleration voltage of 300kV.

Immediately after the sputter deposition, UV–Vis absorption spectra were measured with a spectral photometer (U-3900H, HITACHI Co., Ltd.) with a quartz sample cell of 0.05– 0.10 mm optical pass. In the data correction process, the absorption spectrum of each neat IL was used as the background absorption.

2.5 Other Measurements

We measured the density and viscosity of the ILs using a density meter (DMA4500, Anton Paar GmbH) and a viscosity meter (AMVn, Anton Paar GmbH), respectively, over a 10–90 °C range.

3 Results and discussion

Hereafter, we mainly show the results from SAXS analyses and discuss the sizes of AuNPs based on them. The results from TEM and UV–Vis analyses are shown in Figs. S1–S4 (ESI) and are used as supplementary or complementary information to the SAXS results.

3.1 Anion Effects Studied by SAXS Experiments

To elucidate the anion effects on the size determination of AuNPs, we selected five types of anions, namely, BF$_4^-$, PF$_6^-$, [OTf]$^-$, [FSA]$^-$, and [TFSA]$^-$, and set the cation to be [C$_4$mim]$^+$.

As a typical example, Fig. 2 displays the scattering profiles of the AuNPs against q, which were generated in the [C$_4$mim][OTf] at different temperatures, after corrections[40] for the intensity fluctuation of incident X-rays, background intensities, and absorption effects. Here, q is the scattering parameter defined by $4\pi\sin\vartheta/\lambda$, where 2ϑ is the scattering angle and λ is the wavelength of the X-ray. The black curves in Fig. 2 are theoretical fitting curves, which were obtained assuming that the AuNPs were spherical and that the size distribution was expressed by Γ distribution.[40] This assumption, that each AuNP was spherical, was consistent with the results from TEM as shown in Fig. S1 (ESI). For clarity, the curves are displaced vertically with successive multiplications by 10. Having chosen the scattering intensity of pure [C$_4$mim][OTf] as the reference, we regard the profiles to be the scattering intensities of the AuNPs themselves. The profiles in Fig. 2 gradually change depending on the temperatures of the capture medium IL, which then reflect the size change of the AuNPs. We note that scattering curves obtained at
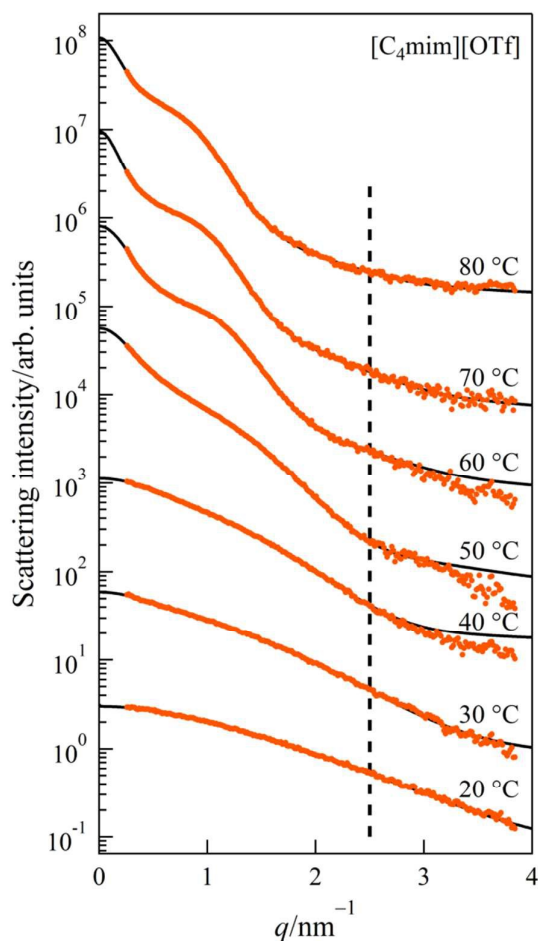
Fig. 2 SAXS profiles of AuNPs generated in [C$_4$mim][OTf] at different temperatures. For clarity, the curves are displaced vertically with successive multiplications by 10. For the fitting analysis, we used data from the smaller q-region to the left of the dashed lines to derive the distribution curves shown in Fig. 3.

Fig. 3 Particle size distributions of AuNPs generated in [C$_4$mim][OTf] at different temperatures.

temperatures higher than 40 °C swell at approximately 0.5 and 1.5 nm^{-1} and the swelling peaks shift to smaller q-values with increases in temperature. The SAXS patterns of the AuNPs generated in the ILs of other anions are shown in Fig. S5 in the ESI.

We fitted the theoretical scattering curves as previously described. The profiles obtained at 20 °C, 30 °C, and 40 °C were well simulated by assuming a simple distribution of spherical NPs. Conversely, experimental curves obtained at temperatures higher than 40 °C with small swellings could be simulated only by assuming interference between the NPs. This indicates that the NPs, at that temperature, start gathering without cohering and the distances between the centers of the NPs increase with increased preparation temperatures. Because the scattering intensity at higher q-regions is very weak and the random variation is large, as shown in Fig. 2, we used the scattering data of smaller q-regions, $0.25 < q < 2.5$ nm^{-1}, to derive the particle size
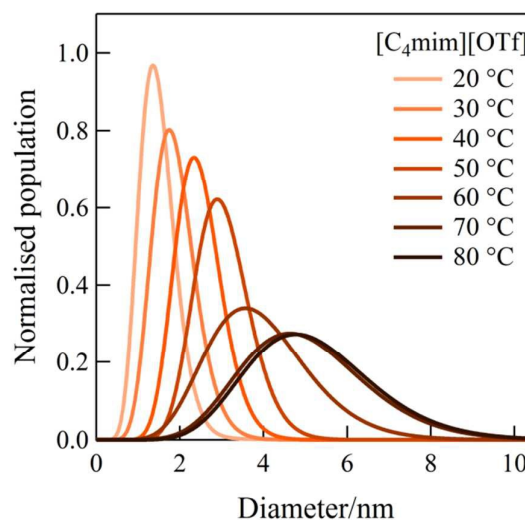
distribution. For the fitting analyses of all other anion cases, we used the same q-region and the results are shown in Fig. S5 (ESI). The theoretical curves are displayed by the black curves and simulate the experimental intensities very well in the lower q-regions for all samples and all temperature data.

The particle size distributions of AuNPs in [C$_4$mim][OTf], as obtained from the results of the abovementioned curve fitting, are shown in Fig. 3. Size distribution curves of the AuNPs in the ILs of other anions are shown in Fig. S6 in the ESI. Although AuNPs generated in [C$_4$mim]BF$_4$ were reported in our previous papers,[40,42] we performed the experiments again on this sample to address the anion effects under the same experimental conditions for all the ILs. The results for the [C$_4$mim]BF$_4$ series in this study are almost identical to those in our previous study,[42] but for the temperature effect of the Au target.[44] The curves indicate the distributions of the number of particles vs. diameter, and they are normalized by area for comparing their distribution widths. As previously described, we extracted two kinds of values from the distribution curve, namely, the value of the diameter at the peak (D_{peak}) and the full width at half maximum (W_{fwhm}) of the distribution curve. The D_{peak} value corresponds to the diameter of the most abundant NPs in the capture medium.

In Fig. 4a and 4b, the values of D_{peak} and W_{fwhm} for the AuNPs generated in the five types of ILs are plotted against the temperature of the ILs, respectively. For all subsequent figures, we indicate the IL capture media of different anions using the same symbols as those used in Fig. 4.

From Fig. 4, we summarize the SAXS results for the AuNPs as follows. First, the size and size distribution of AuNPs differ greatly, depending on the type of anion used in the capture media ILs. Second, excepting the PF$_6^-$ case, the values of both D_{peak} and W_{fwhm} are strongly dependent on the temperature of the capture medium IL and increase as the temperature rises. Conversely, the D_{peak} values of the AuNPs generated in [C$_4$mim]PF$_6$ are exceptional in their nearly constant
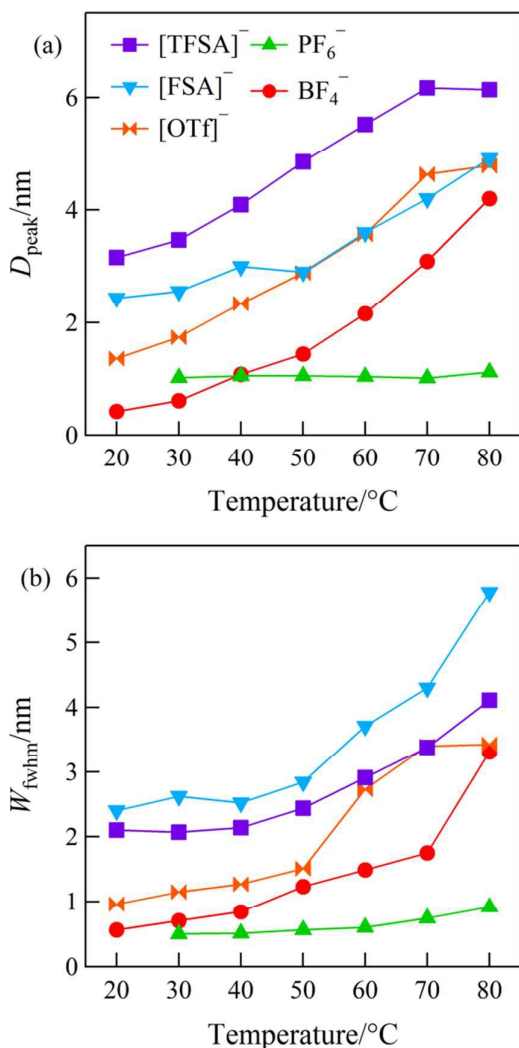
Fig. 4 Dependences on preparation temperature of (a) the diameter values at the peaks and (b) the values of the full width at half maxima for AuNPs generated in the five types of ILs, [C$_4$mim]X (X: BF$_4$, PF$_6$, [OTf], [FSA], and [TFSA]).

independence from temperature, and the W_{fwhm} value increases only a little as temperature rises. Third, the sizes of the AuNPs generated in [C$_4$mim]BF$_4$, [C$_4$mim]PF$_6$, and [C$_4$mim]OTf are relatively uniform at lower temperatures, independent of the type of anion. The first result implies that anion effects are the most important factor in determining the size of NPs. Specifically, anions seems to stabilize the AuNPs to form the first shell. This idea has also been proposed by Janiak et al. for metal NPs prepared by thermal decomposition and reduction of precursors,[37,61] and then cations surround them. The details are discussed in section **3.3** below.

Among the studies addressing AuNP sizes prepared in ILs by the sputter-deposition technique, the results by Wender et al.[43] are appropriate for comparison with our present results. This is because the authors synthesized AuNPs under several experimental conditions to take into account possible size-

determining factors. Some of their capture media correspond to the samples used in our study, namely, [C$_4$mim]BF$_4$, [C$_4$mim]PF$_6$, and [C$_4$mim][TFSA]. Therefore, it is possible to compare the present study with theirs, especially focusing on the anion effects. There are some differences between our results and conclusion and theirs. For example, we confirmed the formation of AuNPs with very small sizes, less than or equal to approximately 1 nm in diameter, in contrast with their sizes of 3.2–4.6 nm.[43] This seems to be caused by the difference in the caracterization methods, namely our method of SAXS and their one of TEM. TEM observations require that preparative operations be made for the sample, which could lead to growth or aggregation of smaller NPs. Conversely, SAXS measurements applied in the present study require no preparative steps and can be performed immediately after the generation of NPs. It is well known that small NPs of 1 nm order are very active and easily aggregate with each other. Moreover, the TEM method is not powerful in the characterizing NPs less than or equal to 1 nm in size. For these reasons, the SAXS experiment is thought to be the most appropriate method for determining the size of smaller NPs dispersed in a medium. The UV–Vis spectra also support the definite existence of AuNPs with very small sizes. Namely, for the AuNPs whose sizes were determined to be less than or equal to 1 nm by SAXS analyses, the surface plasmon resonance (SPR) bands around 520 nm disappeared as shown in Figs. S2–4 in ESI. Moreover, we observed visible photoluminescence from AuNPs generated in [C$_4$mim]PF$_6$,[60] which is characteristic to smaller AuNPs than approximately 1nm.

The greatest difference is that Wender et al. concluded that there was no anion effect in determination of AuNP size. This conclusion seems to be drawn from their experiments in uncontrolled experimental conditions. We revealed that the temperature of a capture medium is the most important size-determining factor in the same year[42] as their report.[43] The effects of the sputtering conditions was also reported in the next year.[44] They obtained AuNPs with almost the same sizes in the ILs with different anions. Their results seem to be caused by no regulation of temperature of the capture medium. If not regulated, the temperature of the capture medium would rise during the deposition and it should lead to generation of AuNPs with various sizes characteristic to the temperatures. On the other hand, present results confirm that the sizes of the prepared AuNPs are definitely affected by the types of anions under maintaining the experimental conditions relating to the size-determining factors constant.

3.2 Revisiting the Effects of Alkyl-Chain Length of Cations

To elucidate the cation effects on the size-determination of AuNPs, we selected four types of imidazolium-based cations with different alkyl-chain lengths, namely, [C$_2$mim]$^+$, [C$_4$mim]$^+$, and [C$_8$mim]$^+$ for BF$_4^-$ as the counter anion and [C$_2$mim]$^+$, [C$_4$mim]$^+$, and [C$_6$mim]$^+$ for [OTf]$^-$. We have previously reported results for the three BF$_4^-$ salts.[40] However, because these were our first experiments for AuNPs generated by the sputter-deposition technique, we had few ideas regarding size-control factors. Subsequent to this report,[40] we have

performed many systematic experiments and proved that the temperature of the capture medium and some sputtering conditions strongly affect the size and size distribution of AuNPs.[42,44] Keeping other size-determination factors constant, we again synthesized AuNPs in $[C_2mim]BF_4$, $[C_4mim]BF_4$, and $[C_8mim]BF_4$. In the present experiments, we also studied the dependence on temperature of the capture IL. With respect to the three $[OTf]^-$ salts incorporated with $[C_2mim]^+$, $[C_4mim]^+$, and $[C_6mim]^+$, the present study is our first trial.

The D_{peak} temperature dependences of AuNPs generated in BF_4^- salts are shown in Fig. 5a. The SAXS patterns and the size distribution curves are shown in Figs. S7 and S8 in ESI, respectively. As shown Fig. 5a, the sizes of the NPs generated in the three ILs are almost identical, independent of the IL types in lower temperatures up to 40 °C. The D_{peak} values for the three ILs increase gently from 20–40 °C, and then increase

sharply with continued increases in temperature. The increasing trends differ depending on the type of IL. Specifically, larger NPs formed in the IL with a shorter alkyl chain. As shown in our report on the temperature effect on the size of AuNPs in $[C_4mim]BF_4$,[42] 50–55 °C is the boundary temperature for which cohesion of the smaller NPs, once generated and stabilized, occurs easily to generate larger NPs. Thus, we conclude that NPs generated at lower temperatures are almost identical in size, independent of the length of the alkyl chain of the imidazolium cations, as represented by the D_{peak} values (Fig. 5a). At higher temperatures, cohesion of the once-generated NPs occurs. This process may differ depending on the stabilization ability of the cations surrounding the once-generated NPs enclosed with a BF_4^- anion. The longer chains seem to work more effectively as stabilizers, and thereby restrict the cohesion of NPs in the IL with the longer alkyl chain. Consequently, the size of AuNPs in an IL with a longer alkyl chain is smaller at higher temperatures.

In previous studies,[40] we performed sputter deposition at room temperature with no temperature control of the capture medium. In the resulting paper, we reported that smaller NPs were generated in the IL with the longer alkyl chain even at lower temperatures, which is different from our present results. We explain this difference as follows. In our earlier study, the temperature of the IL of the capture medium rose during sputtering deposition; consequently, the NPs generated without temperature control were mixtures of NPs generated at various temperatures. Thus, the apparent size of the NPs reported in our previous study showed cation dependence,[40] and this apparent effect would have been manifested to a greater degree for the cation with a shorter alkyl chain.

The D_{peak} temperature dependences of AuNPs generated in $[OTf]^-$ salts are shown in Fig. 5b. As in the case of the BF_4^- system, particle size shows a slight dependence on alkyl-chain length at lower temperatures and the difference between them becomes more distinct as the temperature rises. We believe the same mechanism is operating in the determination of particle size as mentioned above for the $[C_nmim]BF_4$ cases. Specifically, $[OTf]^-$ ions seem to stabilize the AuNPs to form the first shell and then cations surround them. For the $[OTf]^-$ salts, the temperature at which the alkyl-chain length effect appears is lower than that for the BF_4^- salts. We consider that this is because the stabilization ability of $[OTf]^-$ may be weaker than in BF_4^- and the stabilization ability of the cation is evident at lower temperatures in $[OTf]^-$ salts.

3.3 Comparison of Anion and Cation Effects on the Size of AuNPs

Considering the results presented in sections **3.1** and **3.2**, we can definitely conclude that anions have stronger effects than cations on the determination of the size of AuNPs generated in ILs by the sputter-deposition technique. Therefore, we also conclude that the stabilization mechanism of NPs is caused by the enclosure of AuNPs by anions as the first shell, which is similar to the model proposed by Vollmer and Janiak.[37,61] We can also prove that the second shell is the more positively charged moiety of the cations and that the imidazolium ring and long alkyl chains stick out, as shown in Fig. 6.

A similar stabilization model was proposed by Dupont and
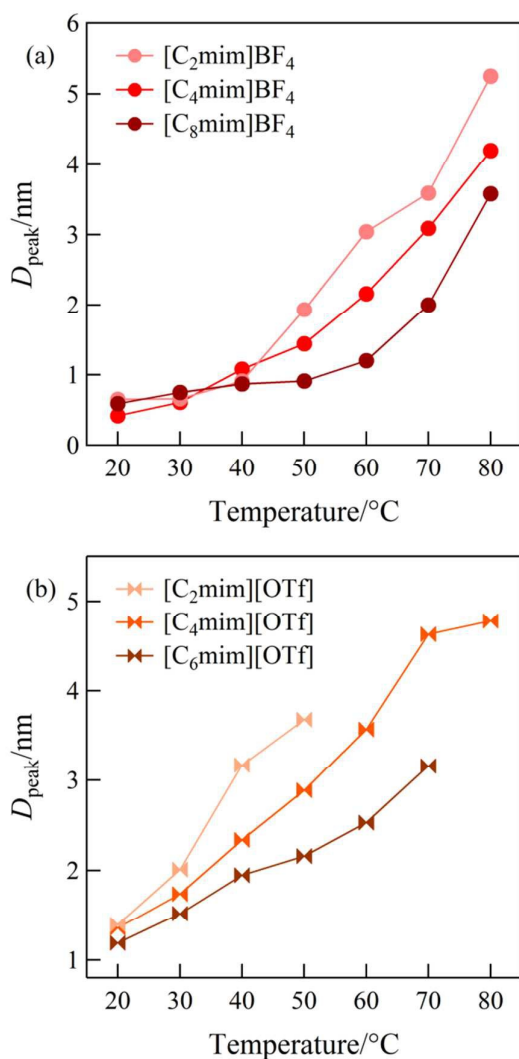
Fig. 5 The diameter values at the peaks in the particle size distributions of AuNPs generated in (a) BF_4^- salts and (b) $[OTf]^-$ salts.
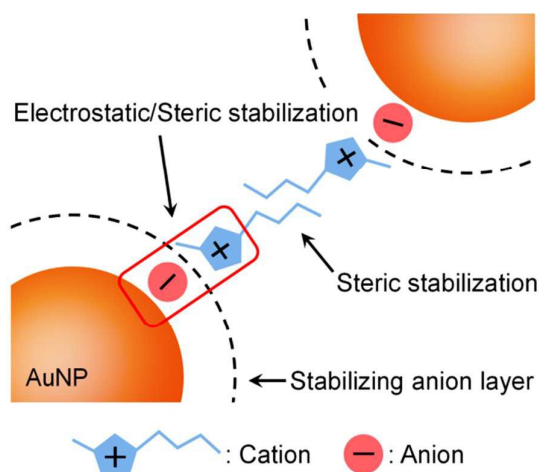
Fig. 6 Model of the stabilization structure in imidazolium-based ILs. Alkyl chains of imidazolium cations have a role in steric stabilization.

Scholten for NPs prepared by chemical reduction in ILs.[36] In their stabilization model, small metal NPs (1–10 nm) in an IL tend to interact with anionic aggregates of the IL. Although the methods of preparing the NPs differ (sputter-deposition technique vs. chemical reaction), the media for dispersing the NPs are the same ILs. Considering that the surface of a metal NP is mostly electron-deficient,[62] we may inevitably conclude that the anions stabilize the NPs and are the most important factor in determining the size of NPs in ILs. Our present results demonstrate this conclusion on the anion effects most definitely. It has been suggested that the stabilization of chemically synthesized metal NPs in ILs is due to the electric double layer on the surface of the particles.[13,62,63] For physically synthesized metal NPs, the first layer is also formed by anions and the second coordination shell seems to be formed by the $[C_4mim]^+$ cations. Regardless of the different generation methods, the results from using both sputter deposition and chemical reaction in ILs support the concept of a stabilization mechanism in the electric double-layer model.

3.4 Temperature Effects on the size of AuNPs

Because the anions dominantly affect the determination of size and size distribution of AuNPs generated by the sputter-deposition technique, hereafter, we mainly focus on five types of anions.

In the previous study wherein we fixed $[C_4mim]BF_4$ as the capture medium, we showed that the temperature of the medium greatly influences the size determination of NPs in the IL. We have previously suggested that this temperature effect is directly connected to the diffusion of Au atoms or clusters that are ejected into the IL.[42] In the present experimental conditions, we think it likely that most of the sputtered particles are not Au clusters but Au atoms.[64]

After deposition on the surface of the IL, Au atoms start dispersing into the liquid. At that time, the diffusion velocity, which is related to the viscosity of the IL, will influence the aggregation processes. In general, the viscosities of ILs drastically change depending on temperature. According to

the Stokes–Einstein relationship, the diffusion constant D of a particle in a medium is given by

$$D = k_B T / 6\pi r\eta, \qquad (1)$$

where η is the viscosity of the medium, k_B is the Boltzmann constant, T is the absolute temperature, and r is the hydrodynamic radius of the particle. D_{peak} and W_{fwhm} plots against T/η for the five ILs with different anions are shown in Figs. 7a and 7b, respectively. We measured the densities and viscosities of the ILs to derive the T/η values, which are plotted in Figs. S9 and S10 in ESI, respectively. For all the samples except $[C_4mim]PF_6$, the graphs show positive relationships between D_{peak} and T/η. As the atoms and small clusters disperse faster in a medium with lower viscosity, they easily collide with each other to form NPs. In this way, larger NPs are generated in a capture medium with lower viscosity, namely, at a higher temperature. More specifically, the positive relationship between D_{peak} and T/η suggests that the main mechanism for NP growth is the collision and subsequent aggregation of Au atoms and small clusters in the ILs.

As shown in Fig. 7a and 7b, the curves of D_{peak} and W_{fwhm} vs. T/η differ individually and we cannot draw a master curve independent of IL type. This result proves that the interaction between Au and anions is another important factor in determining the size of NPs, while collision frequency is also a definite factor for a fixed IL. As such, the formation of NPs is mainly determined by the valance between the collision frequencies of sputtered Au atoms and the stabilization by the coordination of the anions in the first shell, and of the cations (including the alkyl chain) in the second shell.

3.5 Stabilization Factors of Anions

In this section, we focus our attention on determining the type of anions and the specific anion characteristics that act as size-control factors of AuNPs. To summarize the discussion thus far, in section **3.2**, on the basis of the experimental results of the BF_4^- salts and $[OTf]^-$ salts, we showed that the effect of the alkyl-chain lengths of cations is small enough to be neglected in the lower temperature region. In our previous report on the temperature effect, we showed that AuNPs prepared at higher temperatures seem to have experienced a heating effect after their generation.[42] Thus, we can discuss the selective effect of anions in the first stage of AuNP generation by using data from the lower temperature region. Therefore, our next task is to check whether a relationship exists between the anion features and the D_{peak} of AuNPs prepared at the lowest temperatures in the present experiments.

First, we consider the negative-charge distribution of the anion atoms, because it is well known that AuNP surfaces are electron-deficient.[62] Examples where this idea was applicable included Pt and Ir NPs in ILs.[63,65] In the case of BF_4^- and PF_6^-, fluorine atoms have partial negative charges.[66,67] Conversely, the negative-charge distribution in $[OTf]^-$, $[FSA]^-$, and $[TFSA]^-$ ions strongly localize on the oxygen and nitrogen atoms.[68,69] Although it was discussed that the fluorine atoms of the anion (BF_4^-) interacted with the surface of the AuNPs,[61] we found no systematic correlation between the partially distributed negative charge on the atoms in the anions used for preparation and the size of the generated AuNPs. Therefore,
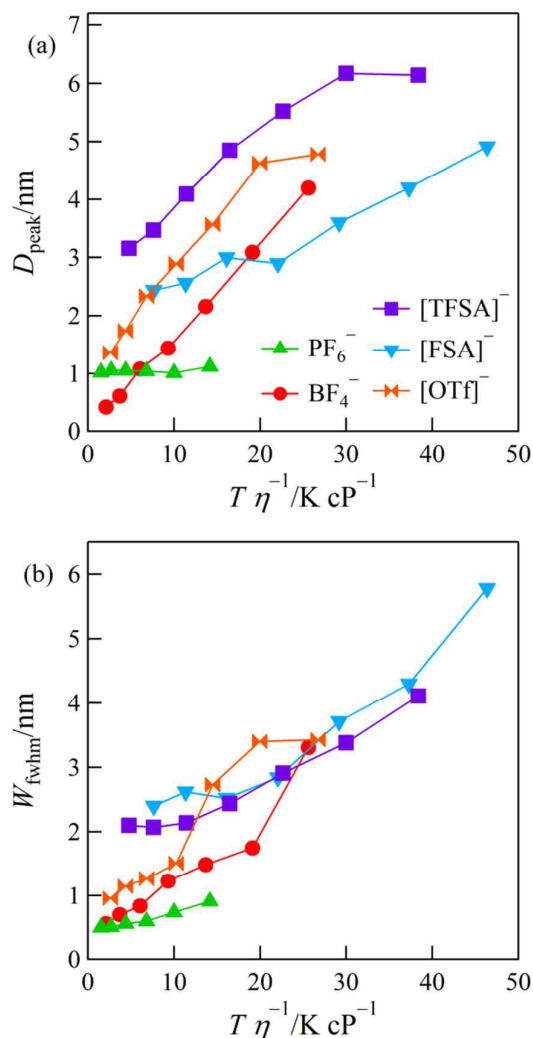
Fig. 7 T/η dependences of (a) the diameter values at the peaks and (b) the full widths at half maxima, extracted from the particle size distributions of AuNPs synthesized in the five types of ILs, $[C_4mim]X$ (X: BF_4, PF_6, [OTf], [FSA], and [TFSA]).

we cannot explain our experimental results by assuming that the charge of specific atoms in the anions are an important factor in determining the formation process and the final size of AuNPs. Although the surface atoms of AuNPs may, of course, be sensitive to the existence of the charges of specific atoms in the first coordinated shell, the partially distributed negative charges do not play a role in size control.

Although we also considered the contribution of the anion donor strengths,[70] we found no systematic relationship between the size of AuNPs and the anion nucleophilicity.

Therefore, in the next step, we examine anion size, which has been reported by Janiak et al. as being a size-control factor in the synthesis of various metal NPs by thermal decomposition and the reduction process from metallic salts or metal carbonyl precursors in ILs.[37,71,72] The authors reported the sizes of their AgNPs to be strongly affected by and bear a

proportional relationship to the volumes of anions.[71] We have also thought that the sizes of anions might be a size-control factor with respect to the sputter-deposition technique for AuNPs. To confirm this idea, we plotted the values of D_{peak} at the lowest preparation temperature against the volume of anions, as shown in Fig. 8. Each error bar in Fig. 8 indicates the value of the W_{fwhm} of the corresponding distribution curve. The values of D_{peak} are clearly proportional to the volumes of anions, in the same manner as chemically generated AgNPs,[71] and thus there is no question that the size of anions is also an important size-control factor in the generation of AuNPs in ILs by sputter deposition. On the basis of the Derjaguin-Landau-Verwey-Overbeek (DLVO) theory,[73,74] Janiak et al. pointed out the importance of the thickness of the first stabilizing shell around an AgNP.[71] We agree with their discussion. Moreover, for our AuNPs, we also take notice on the valance of the volumes between an anion and an AuNP. In the present experiments, subnanometer-sized AuNPs were prepared. While an AuNP of this size is surrounded and stabilized by several smaller BF_4^- ions, it is impossible for it to be efficiently enclosed by larger plural anions such as [TFSA]$^-$. As such, we consider the contributing anion effects to be anion thickness in the electric double layer and the valance of largeness in a surrounded AuNP.

3.6 Where Do Nucleation and Growth of NPs Occur?

The Ar^+ sputtering of Au is known to cause the physical ejection of Au atoms and/or small clusters. As mentioned above, in the present experimental conditions, most of these sputtered particles are Au atoms.[64] As shown in Figs. 3, 4a, and 7a, the sizes of AuNPs differ in different capture media. If we note the type of IL, the NPs increase their size as a function of the temperature of the IL. These facts indicate that the nucleation and growth of NPs occur by aggregation of the
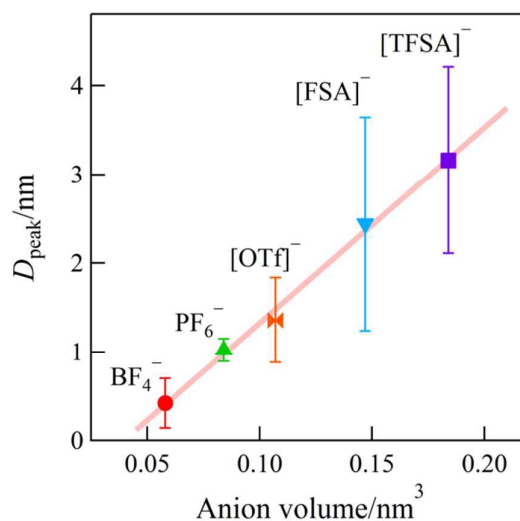
Fig. 8 Relationship between the volume of anions and diameter value at the peak extracted from the particle size distribution of AuNPs synthesized at the lowest preparation temperature in each IL.

sputtered Au atoms after making contact with the temperature-controlled IL. As shown in our previous papers,[42,44] the final concentration after the dispersion of Au into the IL is not the ultimate determining factor of particle size. We also checked that the NPs, once generated, do not change their size and distribution by diluting the solution.[40] The results show that the aggregation of sputtered Au atoms occurs on the surface of the IL and/or at the beginning of the Au dispersion into the IL. So, we now focus our attention on these two candidates—the surface of the IL and the immediate inside surface—as the sites where NP nucleation and growth occur.

The Au atoms generated by the Ar^+ sputtering are first deposited on the surface of the IL. Therefore, the surface tension of the IL seems to influence the formation of AuNPs to some extent. We now consider the effect of IL surface tension. For all the ILs, the surface tensions decrease slightly with a rise in temperature.[75,76] However, the changes seem too small to cause any drastic change in the sizes of the NPs. We considered that the surface tension will determine the staying time of the deposited Au atoms, which will be longer on an IL surface with a higher surface tension. If the staying time were the most significant factor in the aggregation of the deposited Au atoms on the surface of the IL, the NPs generated at higher temperatures (lower surface tension) would become smaller. However, the experimental results with respect to the temperature dependence of the sizes reveal the exact opposite. This shows that surface tension is not a significant factor in determining the size of NPs. Moreover, the most definite evidence that excludes the possibility of the occurrence of NPs on the surface is the following experimental result. Namely, the variation in the discharge current during sputtering causes no difference in the size of AuNPs.[44] This means that the sizes of NPs are independent of the density of the Au atoms deposited on the surface of ILs. These results suggest that from the macroscopic viewpoint, the nucleation and growth of AuNPs do not occur on the surface of ILs.

Next, our discussion takes the microscopic viewpoint. From this standpoint, it is necessary to consider the structural organization of the IL at its surface. It has been reported that both cations and anions are present in the surface region of pure imidazolium-based ILs with short alkyl chains such as $[C_2mim]^+$.[77] For the cations of imidazolium-based ILs with longer alkyl chains (i.e., $[C_4mim]^+$, $[C_6mim]^+$, and $[C_8mim]^+$ in the present case), the alkyl chains tend to project out from the surface into the gas or vacuum phase to be lined up. In contrast, the ionic aspect of the charged imidazolium rings or anions tend to stay on the inner surface of the bulk liquid phase.[78-80] If nucleation and growth occur on the nonpolar region formed by the alkyl chains, differences in the alkyl-chain length of ILs should influence the size of AuNPs. However, the sizes of NPs generated in BF_4^- salts or $[OTf]^-$ salts at lower temperatures are almost identical. Therefore, we can only conclude that the projecting region of alkyl chains is not where the nucleation and growth of AuNPs takes place.

The composition of ILs on the immediate inner surface may be a key factor in the size control of AuNPs. It has been

reported that the composition of the immediate inner surface of imidazolium-based ILs with a long alkyl chain is dependent on the anion. In particular, the constitutions of alkyl side chains and fluorinated anions on the inner surface are $PF_6^- - BF_4^- > [TSFA]^-$.[81,82] Although the inner surface compositions of PF_6^- and BF_4^- are very similar, our experimental results show that the size-distributions of AuNPs generated in these corresponding ILs differ.

Considering our present experimental results and the surface structures of ILs, we must deny the possibility that nucleation and growth occurs on the surface of capture media ILs. This conclusion is in disagreement with that of Wender et al.[43] We believe that the authors drew their conclusions on the basis of experimental results that were obtained from unregulated experimental conditions, as discussed in section **3.1**. In summary, our results lead us conclude that the nucleation and growth of AuNPs may possibly occur inside the ILs, just slightly away from the surface. As discussed above, ions, and especially anions, work as stabilizers in NPs. The nucleation and growth of NPs progress by the collision of Au atoms and small clusters, and stabilization by the coordination of the anions and cations stops the NP growth. The sizes of NPs are determined by the balance of the collision and stabilization activity. We think this valance comes into play when Au atoms begin to diffuse into the ILs. We also think that the region of its occurrence may not be the first layer of the inner surface but a more inner region, where Au atoms and ions can defuse freely. This is because the growth and growth cessation of NPs are strongly affected by the AuNPs collisions and the stabilization by ions. The size of the generated AuNPs is strongly influenced not by the organized structure of the surface but rather the bulk property and structure of each IL.

Conclusions

To elucidate the size-control factors of AuNPs prepared by sputter deposition in ILs, we performed experiments for nine kinds of ILs as the capture media, while changing the preparation temperature from 20 to 80 °C. In particular, we focused on the anion and cation effects and preparation temperature effects for each IL. We derived the size-distribution curve of the AuNPs prepared in each IL and at each temperature by a curve-fitting analysis of the corresponding SAXS patterns.

Except for the AuNPs prepared in $[C_4mim]PF_6$, our results show that the size and size distribution of AuNPs increase with the temperature of the capture medium. In every type of anion, the AuNPs prepared in the ILs ($[C_4mim]X$, X^-: BF_4^-, PF_6^-, $[OTf]^-$, $[FSA]^-$, and $[TFSA]^-$) exhibit different D_{peak} and W_{fwhm} values and temperature dependences. Conversely, the sizes of AuNPs, prepared in BF_4^- salts or $[OTf]^-$ salts with different alkyl-chain lengths in the imidazolium-based cations, are nearly the same in lower preparation temperatures and alkyl-chain length effects appear only at higher temperatures. These experimental results show that the anions enclose AuNPs and stabilize them by forming the first shell, and the cations form the second shell.

The sizes of AuNPs prepared at the lowest preparation temperature exhibit a close relationship with the anion's volumes in the capture media ILs. We conclude that the size of AuNPs is determined by the balance of the collision frequencies of ejected Au atoms and the stabilization power of the anions. The volume of anions is regarded as the most important factor in determining AuNP size. The anion volume relates to the thickness of the electric double layer. The balance between the bulkiness of the anion and that of the enclosed AuNP is also an important factor in determining the size.

Acknowledgements

References

1. C. J. Murphy, T. K. Sau, A. M. Gole, C. J. Orendorff, J. Gao, L. Gou, S. E. Hunyadi and T. Li, *J. Phys. Chem. B*, 2005, **109**, 13857–13870.
2. M. E. Stewart, C. R. Anderton, L. B. Thompson, J. Maria, S. K. Gray, J. A. Rogers and R. G. Nuzzo, *Chem. Rev.*, 2008, **108**, 494–521.
3. V. Biju, T. Itoh, A. Anas, A. Sujith and M. Ishikawa, *Anal. Bioanal. Chem.*, 2008, **391**, 2469–2495.
4. D. V. Talapin, J.-S. Lee, M. V. Kovalenko and E. V. Shevchenko, *Chem. Rev.*, 2010, **110**, 389–458.
5. R. Ferrando, J. Jellinek and R. L. Johnston, *Chem. Rev.*, 2008, **108**, 845–810.
6. K. Saha, S. S. Agasti, C. Kim, X. Li and V. M. Rotello, *Chem. Rev.*, 2012, **112**, 2739–2779.
7. J. M. Campelo, D. Luna, R. Luque, J. M. Marinas and A. A. Romero, *ChemSusChem*, 2009, **2**, 18–45.
8. C.-J. Jia and F. Schuth, *Phys. Chem. Chem. Phys.*, 2011, **13**, 2457–2487.
9. D. Astruc, F. Lu and J. R. Aranzaes, *Angew. Chem. Int. Ed.*, 2005, **44**, 7852–7872.
10. C. Burda, X. Chen, R. Narayanan and M. A. El-Sayed, *Chem. Rev.*, 2005, **105**, 1025–1102.
11. J. P. Wilcoxon and B. L. Abrams, *Chem. Soc. Rev.*, 2006, **35**, 1162–1194.
12. J. Dupont, G. S. Fonseca, A. P. Umpierre, P. F. P. Fichtner and S. R. Teixeira, *J. Am. Chem. Soc.*, 2002, **124**, 4228–4229.
13. P. Migowski and J. Dupont, *Chem. Eur. J.*, 2007, **13**, 32–39.
14. Y. Wang and H. Yang, *J. Am. Chem. Soc.*, 2005, **127**, 5316–5317.
15. Y. Yu, Q. Sun, X. Liu, H. Wu, T. Zhou and G. Shi, *Chem. Eur. J.*, 2011, **17**, 11314–11323.
16. Z. He and P. Alexandridis, *Phys. Chem. Chem. Phys.*, 2015, **17**, 18238–18261.
17. C. Janiak, *Z. Naturforsch. B*, 2013, **68**, 1059–1089.
18. C. Janiak, in *Catalysis in Ionic Liquids: From Catalyst Synthesis to Application*, Eds. C. Hardacre and V. Parvulescu, RSC Publishing, Cambridge, 2014, ch. 11, pp. 537–577.
19. C. Janiak, in *Ionic Liquids in Organometallic Catalysis*, eds. J. Dupont and L. Kollár, Springer, Berlin Heidelberg, 2015, vol. 51, ch. 70, pp. 17–53.
20. S. Kuwabata, T. Tsuda and T. Torimoto, *J. Phys. Chem. Lett.* 2010, **1**, 3177–3188.
21. K. R. J. Lovelock, *Phys. Chem. Chem. Phys.*, 2012, **14**, 5071–5089.
22. T. Torimoto, K. Okazaki, T. Kiyama, K. Hirahara, N. Tanaka and S. Kuwabata, *Appl. Phys. Lett.*, 2006, **89**, 243117.
23. K. Okazaki, T. Kiyama, K. Hirahara, N. Tanaka, S. Kuwabata and T. Torimoto, *Chem. Commun.*, 2008, 691–693.
24. S. Suzuki, T. Suzuki, Y. Tomita, M. Hirano, K. Okazaki, S. Kuwabata and T. Torimoto, *CrystEngComm*, 2012, **14**, 4922–4926.
25. S. Suzuki, Y. Tomita, S. Kuwabata and T. Torimoto, *Dalton Trans.*, 2015, **44**, 4186–4194.
26. K. Richter, A. Birkner and A.-V. Mudring, *Angew. Chem. Int. Ed.*, 2010, **49**, 2431–2435.
27. K. Richter, A. Birkner and A.-V. Mudring, *Phys. Chem. Chem. Phys.*, 2011, **13**, 7136–7141.
28. K. Richter, P. S. Campbell, T. Baecker, A. Schimitzek, D. Yaprak and A.-V. Mudring, *Phys. Status Solidi B*, 2013, **250**, 1152–1164.
29. Y. Kimura, H. Takata, M. Terazima, T. Ogawa and S. Isoda, *Chem. Lett.*, 2007, **36**, 1130–1131.
30. H. Wender, M. L. Andreazza, R. R. B. Correia, S. R. Teixeira and J. Dupont, *Nanoscale*, 2011, **3**, 1240–1245.
31. M. J. Earle, J. M. S. S. Esperanca, M. A. Gilea, J. N. Canongia Lopes, L. P. N. Rebelo, J. W. Magee, K. R. Seddon and J. A. Widegren, *Nature*, 2006, **439**, 831–834.
32. J. M. S. S. Esperança, J. N. C. Lopes, M. Tariq, L. M. N. B. F. Santos, J. W. Magee and L. P. N. Rebelo, *J. Chem. Eng. Data*, 2010, **55**, 3–12.
33. I. Nakatani, T. Furubayashi, T. Takahashi and H. Hanaoka, *J. Magn. Magn. Mater.*, 1987, **65**, 261–264.
34. M. Wagener and B. Günther, *J. Magn. Magn. Mater.*, 1999, **201**, 41–44.
35. S. Stoeva, K. J. Klabunde, C. M. Sorensen and I. Dragieva, *J. Am. Chem. Soc.*, 2002, **124**, 2305–2311.
36. J. Dupont and J. D. Scholten, *Chem. Soc. Rev.*, 2010, **39**, 1780–1804.
37. C. Vollmer and C. Janiak, *Coord. Chem. Rev.*, 2011, **255**, 2039–2057.
38. K. Okazaki, T. Kiyama, T. Suzuki, S. Kuwabata and T. Torimoto, *Chem. Lett.*, 2009, **38**, 330–331.
39. T. Suzuki, K. Okazaki, T. Kiyama, S. Kuwabata and T. Torimoto, *Electrochemistry*, 2009, **77**, 636–638.
40. Y. Hatakeyama, M. Okamoto, T. Torimoto, S. Kuwabata and K. Nishikawa, *J. Phys. Chem. C*, 2009, **113**, 3917–3922.
41. T. Kameyama, Y. Ohno, T. Kurimoto, K. Okazaki, T. Uematsu, S. Kuwabata and T. Torimoto, *Phys. Chem. Chem. Phys.*, 2010, **12**, 1804–1811.
42. Y. Hatakeyama, S. Takahashi and K. Nishikawa, *J. Phys. Chem. C*, 2010, **114**, 11098–11102.
43. H. Wender, L. F. Oliveira, P. Migowski, A. F. Feil, E. Lissner, M. H. G. Prechtl, S. R. Teixeira and J. Dupont, *J. Phys. Chem. C*, 2010, **114**, 11764–11768.
44. Y. Hatakeyama, K. Onishi and K. Nishikawa, *RSC Adv.*, 2011, **1**, 1815–1821.
45. Y. Shishino, T. Yonezawa, K. Kawai and H. Nishihara, *Chem. Commun.*, 2010, **46**, 7211–7213.
46. H. Wender, P. Migowski, A. F. Feil, L. F. Oliveira, M. H. G. Prechtl, R. Leal, G. Machado, S. R. Teixeira and J. Dupont, *Phys. Chem. Chem. Phys*, 2011, **13**, 13552–13557.
47. H. Wender, L. F. Oliveira, A. F. Feil, E. Lissner, P. Migowski, M. R. Meneghetti, S. R. Teixeira and J. Dupont, *Chem. Commun.*, 2010, **46**, 7019–7021.
48. Y. Shishino, T. Yonezawa, S. Udagawa, K. Hase and H. Nishihara, *Angew. Chem. Int. Ed.*, 2011, **50**, 703–705.
49. Y. Hatakeyama, T. Morita, S. Takahashi, K. Onishi and K. Nishikawa, *J. Phys. Chem. C*, 2011, **115**, 3279–3285.

50. Y. Hatakeyama, J. Kato, T. Mukai, K. Judai and K. Nishikawa, *Bull. Chem. Soc. Jpn.*, 2014, **87**, 773–779.

51. T. Sumi, S. Motono, Y. Ishida, N. Shirahata and T. Yonezawa, *Langmuir*, 2015, **31**, 4323–4329.

52. Y. Ishida, R. Nakabayashi, M. Matsubara and T. Yonezawa, *New J. Chem.*, 2015, **39**, 4227–4230.

53. Y. Hatakeyama, K. Asakura, S. Takahashi, K. Judai and K. Nishikawa, *J. Phys. Chem. C*, 2014, **118**, 27973–27980.

54. C. Lee, W. Yang and R. G. Parr, *Phys. Rev. B*, 1988, **37**, 785–789.

55. A. D. Becke, *J. Chem. Phys.*, 1993, **98**, 5648–5652.

56. M. J. Frisch, G. W. Trucks, H. B. Schlegel, G. E. Scuseria, M. A. Robb, J. R. Cheeseman, G. Scalmani, V. Barone, B. Mennucci, G. A. Petersson, H. Nakatsuji, M. Caricato, X. Li, H. P. Hratchian, A. F. Izmaylov, J. Bloino, G. Zheng, J. L. Sonnenberg, M. Hada, M. Ehara, K. Toyota, R. Fukuda, J. Hasegawa, M. Ishida, T. Nakajima, Y. Honda, O. Kitao, H. Nakai, T. Vreven, J. A. Montgomery, Jr., J. E. Peralta, F. Ogliaro, M. Bearpark, J. J. Heyd, E. Brothers, K. N. Kudin, V. N. Staroverov, R. Kobayashi, J. Normand, K. Raghavachari, A. Rendell, J. C. Burant, S. S. Iyengar, J. Tomasi, M. Cossi, N. Rega, J. M. Millam, M. Klene, J. E. Knox, J. B. Cross, V. Bakken, C. Adamo, J. Jaramillo, R. Gomperts, R. E. Stratmann, O. Yazyev, A. J. Austin, R. Cammi, C. Pomelli, J. W. Ochterski, R. L. Martin, K. Morokuma, V. G. Zakrzewski, G. A. Voth, P. Salvador, J. J. Dannenberg, S. Dapprich, A. D. Daniels, O. Farkas, J. B. Foresman, J. V. Ortiz, J. Cioslowski and D. J. Fox, *Gaussian 09, Revision C.01*, Gaussian Inc., Wallingford CT, 2009.

57. S. Zhang, X. Li, H. Chen, J. Wang, J. Zhang and M. Zhang, *J. Chem. Eng. Data*, 2004, **49**, 760–764.

58. L. A. S. Ries, F. A. Amaral, K. Matos, E. M. A. Martini, M. O. Souza and R. F. Souza, *Polyhedron*, 2008, **27**, 3287–3293.

59. A. M. O'Mahony, D. S. Silvester, L. Aldous, C. Hardacre and R. G. Compton, *J. Chem. Eng. Data*, 2008, **53**, 2884–2891.

60. T. Iimori, Y. Hatakeyama, K. Nishikawa, M. Kato and N. Ohta, *Chem. Phys. Lett.*, 2013, **586**, 100–103.

61. E. Redel, M. Walter, R. Thomann, C. Vollmer, L. Hussein, H. Scherer, M. Kruger and C. Janiak, *Chem. Eur. J.*, 2009, **15**, 10047–10059.

62. S. Özkar and R. G. Finke, *J. Am. Chem. Soc.*, 2002, **124**, 5796–5810.

63. C. W. Scheeren, G. Machado, S. R. Teixeira, J. Morais, J. B. Domingos and J. Dupont, *J. Phys. Chem. B*, 2006, **110**, 13011–13020.

64. W. O. Hofer, in *Sputtering by Particle Bombardment III*, eds. R. Behrisch and K. Wittmaack, Springer, Berlin Heidelberg, 1991, ch. 2, pp. 15–90.

65. G. S. Fonseca, G. Machado, S. R. Teixeira, G. H. Fecher, J. Morais, M. C. M. Alves and J. Dupont, *J. Colloid Interface Sci.*, 2006, **301**, 193–204.

66. C. E. R. Prado and L. C. G. Freitas, *J. Mol. Struct.: THEOCHEM*, 2007, **847**, 93–100.

67. J. N. C. Lopes, J. Deschamps and A. A. H. Pádua, *J. Phys. Chem. B*, 2004, **108**, 2038–2047.

68. J. N. C. Lopes and A. A. H. Pádua, *J. Phys. Chem. B*, 2004, **108**, 16893–16898.

69. J. N. C. Lopes, K. Shimizu, A. A. H. Pádua, Y. Umebayashi, S. Fukuda, K. Fujii and S. Ishiguro, *J. Phys. Chem. B*, 2008, **112**, 9449–9455.

70. M. J. Muldoon, C. M. Gordon and I. R. Dunkin, *J. Chem. Soc., Perkin Trans. 2*, 2001, 433–435.

71. E. Redel, R. Thomann and C. Janiak, *Inorg. Chem.*, 2008, **47**, 14–16.

72. E. Redel, R. Thomann and C. Janiak, *Chem. Commun.*, 2008, 1789–1791.

73. E. J. W. Verwey and J. Th. G. Overbeek, *Theory of the Stability of Lyophobic Colloid*, Elsevier, Amsterdam, 1948.

74. B. W. Ninham, *Adv. Colloid Interface Sci.*, 1999, **83**, 1–17.

75. M. G. Freire, P. J. Carvalho, A. M. Fernandes, I. M. Marrucho, A. J. Queimada and J. A. P. Coutinho, *J. Colloid Interface Sci.*, 2007, **314**, 621–630.

76. M. H. Ghatee and A. R. Zolghadr, *Fluid Phase Equilib.*, 2008, **263**, 168–175.

77. C. S. Santos and S. Baldelli, *J. Phys. Chem. B*, 2007, **111**, 4715–4723.

78. T. Iimori, T. Iwahashi, K. Kanai, K. Seki, J. Sung, D. Kim, H. Hamaguchi and Y. Ouchi, *J. Phys. Chem. B*, 2007, **111**, 4860–4866.

79. T. Iwahashi, T. Miyamae, K. Kanai, K. Seki, D. Kim and Y. Ouchi, *J. Phys. Chem. B*, 2008, **112**, 11936–11941.

80. Y. Jeon, J. Sung, W. Bu, D. Vaknin, Y. Ouchi and D. Kim, *J. Phys. Chem. C*, 2008, **112**, 19649–19654.

81. K. R. J. Lovelock, C. Kolbeck, T. Cremer, N. Paape, P. S. Schulz, P. Wasserscheid, F. Maier and H.-P. Steinrück, *J. Phys. Chem. B*, 2009, **113**, 2854–2864.

82. C. Kolbeck, T. Cremer, K. R. J. Lovelock, N. Paape, P. S. Schulz, P. Wasserscheid, F. Maier and H.-P. Steinrück, *J. Phys. Chem. B*, 2009, **113**, 8682–8688.

Graphical Abstract
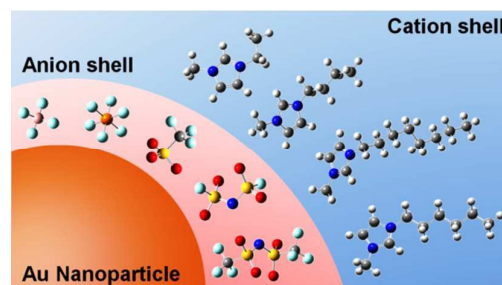
Conceptual diagram of the stabilization structure for AuNPs in imidazolium-based ILs.